J Mol Model (2013) 19:4039–4047
DOI 10.1007/s00894-013-1931-8

ORIGINAL PAPER

DFT study on crystalline 1,1-diamino-2,2-dintroethylene under high pressures

Qiong Wu · Weihua Zhu · Heming Xiao

Received: 10 May 2013 / Accepted: 18 June 2013 / Published online: 20 July 2013

Abstract DFT calculations have been performed to study the structural, electronic, absorption, and thermodynamic properties of crystalline 1,1-diamino-2,2-dintroethylene (α-FOX-7) in the pressure range of 0–40 GPa. A comprehensive analysis of the variation trends of the lattice constants, bond lengths, bond angles, and twist angles under compression shows that six structural transformations occur in α-FOX-7 at 2, 5, 11, 19, 29, and 35 GPa, respectively. The C1-N1 and C1-N2 bond lengths decrease much faster than any other bonds under compression, indicating that the C-NO_2 cleavage is possible to trigger the decomposition of α-FOX-7. The intra-molecular H-bonding interaction weakens at 2 and 5 GPa, which may be caused by the structural transformations, but it then strengthens with the increasing pressure up to 40 GPa. The inter-molecular H-bonding interaction strengthens with the increasing pressure. The band gap of α-FOX-7 increases at 11 GPa suddenly and decreases obviously at 19, 29, and 35 GPa, which are caused by the structural transformations. α-FOX-7 has relatively high optical activity at high pressure. All the structural transformations are endothermic and not spontaneous at room temperature.

Keywords Absorption spectra · Density functional theory · 1,1-diamino-2,2-dintroethylene crystal · Hydrostatic pressure · Structure · Thermodynamic properties

Introduction

1,1-diamino-2,2-dintroethylene (FOX-7, Fig. 1) developed in 1998 [1] is a novel high-energy explosive, which possesses higher performance and lower sensitivity than very known explosive RDX (1,3,5-trinitro-1,3,5-hexahydrotriazine). FOX-7 shows much promise as a potential substitute for famous insensitive explosive TATB (1,3,5-triamino-2,4,6-trinitrobenzene), which was first synthesized as early as 1887 [2]. Many experimental and theoretical studies [3–16] have been done to study the physical and chemical properties of FOX-7 under both normal conditions and extreme conditions since its discovery. It is of great importance to determine the structure and properties of explosives under extreme conditions because the explosives experience extreme high pressure of 50 GPa and high temperature of 5000 K during detonation process [17]. Before the detonation of the explosives, they may undergo phase transitions to form new polymorphs. It is known that different polymorphs of the explosives have different crystal packing which have a great influence on their performances and sensitivity. For instance, HMX (octahydro-1,3,5,7-tetranitro-1,3,5,7-tetrazocin) [18, 19] and RDX [20, 21] both have several polymorphs, which possess different structures and properties. Also, the explosives may take part in decomposition reactions under such extreme conditions. Therefore, to study the structure and behavior of explosives under extreme conditions can provide valuable information for understanding their sensitivity, performance, and safety.

It is reported that FOX-7 undergoes two [15, 16] phase transitions under high temperature. α-FOX-7, which is the most stable phase under ambient temperature and ambient pressure, transforms into β phase at the temperature of around 388 K. Then, a transformation into γ phase occurs at about 435 K. Finally, γ-FOX-7 begins to decompose at 504 K. The three polymorph phases of FOX-7 have been determined and synthesized successfully. However, the study of FOX-7 under high pressure is insufficient and it behavior under high pressure is not very clear still. Although some studies have been done to find some evidences for phase transitions under different pressures, their results are disagreeable with each other. For instance, Peiris et al. [23, 24] reported that α-FOX-7 transforms into a quasi-amorphous phase above 4.5 GPa under nonhydrostatic conditions. The Raman spectroscopy

Q. Wu · W. Zhu (✉) · H. Xiao
Institute for Computation in Molecular and Materials Science and Department of Chemistry, Nanjing University of Science and Technology, Nanjing 210094, China
e-mail: zhuwh@mail.njust.edu.cn

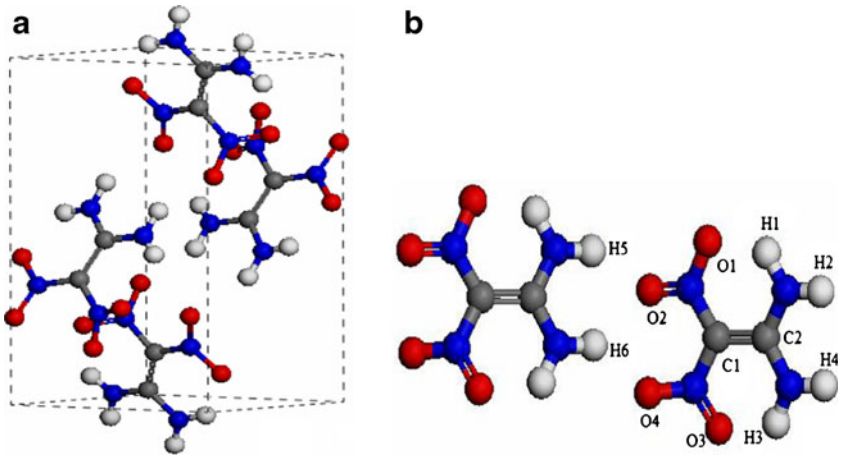

Fig. 1 Crystal and molecular structures of α-FOX-7

studies of FOX-7 under high pressure till 20 GPa [25] show that it may undergo two phase transitions at around 5 GPa and 9–10 GPa, respectively. Zhao et al. [26] performed DFT calculations to study the behavior of FOX-7 till 4 GPa and did not observe any phase transitions. Recently, the high-pressure far- and mid-infrared spectroscopy study of FOX-7 till 28 GPa [22] indicates that it may go through two phase transitions at about 2 and 5 GPa, respectively, and the third one may occur above 10 GPa (or a completion of a phase transition) possibly. In addition, there are no pressure-induced crystals determined and synthesized successfully. Thus, for the reasons above, there is a clear need to further investigate the structure and properties of FOX-7 under high pressures.

The investigation of microscopic properties of energetic materials, which possess a complex chemical behavior, remains a challenging task. Theoretical calculations are an effective way to model the physical and chemical properties of complex solids at the atomic level as a complement to experimental work. Recently, density functional theory (DFT) method with pseudopotentials and a plane-wave basis set has been well-established and has been applied successfully to study the structures and properties of energetic solids under hydrostatic compression [27–30].

In this study, we performed periodic DFT calculations to study the structural, electronic, absorption, and thermodynamic properties of α-FOX-7 crystal under hydrostatic pressure of 0–40 GPa. To investigate the crystal structure at different pressures, the atomic positions and the unit-cell parameters were allowed to relax to the minimum energy. Then we examined their variations in structure and properties under different pressures.

Computational methods

The calculations performed in this study were done within the framework of DFT based on CASTEP code [31], using Vanderbilt-type ultrasoft pseudopotentials [32] and a plane-wave expansion of the wave functions. The self-consistent ground state of the system was determined by using a band-by-band conjugate gradient technique to minimize the total energy of the system with respect to the plane wave coefficients. The electronic wave functions were obtained by using a density-mixing minimization method [33] for the self-consistent field calculation and the structures were relaxed by using the Broyden, Fletcher, Goldfarb, and Shannon (BFGS) [34] method. Geometry optimization is based on reducing the magnitude of calculated forces and stresses until they become smaller than convergence tolerances. Therefore, it is possible to specify an external stress tensor to model the behavior of the system under tension, compression, shear, etc. In these cases the internal stress tensor is iterated until it becomes equal to the applied external stress. The LDA functional proposed by Ceperley and Alder [35] and parameterized by Perdew and Zunder [36], named CA-PZ, was employed. The cutoff energy of plane waves was set to 310 eV. Brillouin zones sampling was performed by using the Monkhost-Pack scheme with a k-point grid of $2\times2\times1$. The values of the kinetic energy cutoff and the k-point grid were determined to ensure the convergence of total energies.

The crystal structure of α-FOX-7 at ambient pressure and temperature was used as input structure. The α-FOX-7 crystallizes in a monoclinic lattice with $P2_1/n$ space group and contains four $C_2H_4N_4O_4$ molecules per unit cell [3]. Figure 1 displays crystal and molecular structures of α-FOX-7. The experimental crystal structure of α-FOX-7 [3] was first relaxed to allow the ionic configurations, cell shape, and volume to change at ambient pressure. Then from this relaxed structure, we applied hydrostatic compression [37, 38] of 1–40 GPa to relax the crystal structure without any symmetry constraints. The pressure is applied equally in all directions. All the calculations are based on the same crystal structure of α-FOX-7. In the geometry relaxation, the total energy of the system was converged less than 2.0×10^{-5} eV,

the residual force less than 0.05 eV/Å, the displacement of atoms less than 0.002 Å, and the residual bulk stress less than 0.1 GPa. Previous studies employing the same approach to simulate the hydrostatic compression of other energetic crystals [39, 40] indicate that the calculated results were in agreement with the experiments.

Results and discussion

Previous studies on energetic molecular crystals [27–29] show that the LDA functional could produce more reliable geometrical structures than the generalized gradient approximation (GGA). As a benchmark, LDA/CA-PZ and GGA/PW91 (Perdew-Wang 91) [41] were selected to fully relax α-FOX-7 crystal at ambient pressure without any constraints. Table 1 presents the experiment and relaxed cell parameters of α-FOX-7 crystal and other theoretical results [26]. It is seen that the errors in the LDZ results are much smaller than those in the GGA results in comparison with the experimental values. Compared with other calculated results [26], it is also found that our LDA results are closer to the experimental values. Thus, the LDA (CA-PZ) method was employed in this study.

Crystal structure

Figure 2a displays the relaxed lattice constants of α-FOX-7 crystal under different hydrostatic pressures. It is found that *a* and *b* decrease gradually as the pressure increases from 0 to 40 GPa. However, the case is a little different for *c*. First, it decreases fast at 1 GPa but increases obviously at 2 GPa. Then it decreases regularly again until 40 GPa. Thus, it may be inferred that α-FOX-7 may undergo structural transformation at 2 GPa, in agreement with experimental reports [22, 25]. More evidence about the structural transformation will be shown below.

Figure 2b presents the compression ratios of the lattice constants (the ratio of the lattice constant at high pressure to that at constant pressure) of α-FOX-7 at different pressures. As the pressure increases, the variation trend of the compression ratios of the lattice constants *a*, *b*, and *c* are quite different, which indicates that the compressibility of α-FOX-7 crystal is anisotropic. When the pressure is below 15 GPa, the compressibilities in the *b*-direction is significantly greater than those in the *a*- and *c*-direction. The compression ratios in different direction follows the sequence of $b > a > c$. When the pressure increases from 0 to 15 GPa, its unit cell is compressed by 5.69 %, 16.85 %, and 5.68 % along the directions of *a*, *b*, and *c*, respectively. This shows that the structure is much stiffer in the *a* and *c* directions than in the *b*-direction. However, in the pressure range of 13-50 GPa, the compressible order along different directions changes to $b > c > a$. When the pressure increases from 16 to 40 GPa, the compression ratios along the directions of *a*, *b*, and *c* are 2.92 %, 6.29 %, and 4.46 %, respectively. In all, the total compression ratios along the directions of *a*, *b*, and *c* in the whole pressure range studied here are 8.61 %, 23.14 %, and 10.14 %, respectively. This means that its structure is much stiffer in the *a* and *c* directions than in the *b* direction.

Figure 2c presents the unit cell angles of α-FOX-7 at different pressures. First, in the pressure range of 0–10 GPa, it decreases gradually and does much more significantly at 2 and 5 GPa. Then it increases obviously at 11 GPa and decreases slowly until 18 GPa but decreases quickly at 19 GPa. In the pressure range of 20–34 GPa, it decreases gradually but increases obviously at 35 GPa. Finally, it decreases gradually until 40 GPa. Thus, it may be concluded that α-FOX-7 goes through five structural transformations at 2 GPa [22, 25], 5 GPa [22, 25], 11 GPa [22], 19 GPa, and 35 GPa, respectively.

The unit cell volume of α-FOX-7 crystal at different pressures is displayed in Fig. 3. Since *a*, *b*, and *c* decrease gradually with the increasing pressure, the unit cell volume decreases monotonically too. It is compressed by 39.9 % in the pressure range of 0–40 GPa.

Molecular structure

Figure 4 displays the bond lengths of α-FOX-7 at different pressures. As the pressure increases, the C-C and four C-N bond lengths decrease gradually, as shown in Fig. 4a. Their total decrease ratios from 0 to 40 GPa are 2.75 %, 3.18 %, 3.08 %, 2.20 %, and 2.34 % for the C1-C2, C1-N1, C1-N2, C2-N3, and C2-N4 bond lengths, respectively. The total decrease ratios of C-NO_2 bond lengths (C1-N1 and C1-N2)

Table 1 Comparison of relaxed lattice parameters of α-FOX-7 with experimental data at ambient condition

Method	*a*(Å)	*b*(Å)	*c*(Å)	β(°)	Cell volume
Expt.	6.934	6.623	11.312	90.06	519.5
LDA/CA-PZ	6.820(−1.64)	6.523(−1.60)	11.106(−1.82)	90.66(0.67)	494.1(−4.89)
GGA/PW91	7.600(9.60)	7.354(11.03)	11.423(0.98)	94.02(4.40)	638.3(22.86)
Ref. [11]	6.74(−2.80)	6.18(−6.69)	11.05(−2.32)	90.7(0.71)	460.5(11.36)

The values in parentheses correspond to the percentage differences relative to the experimental data

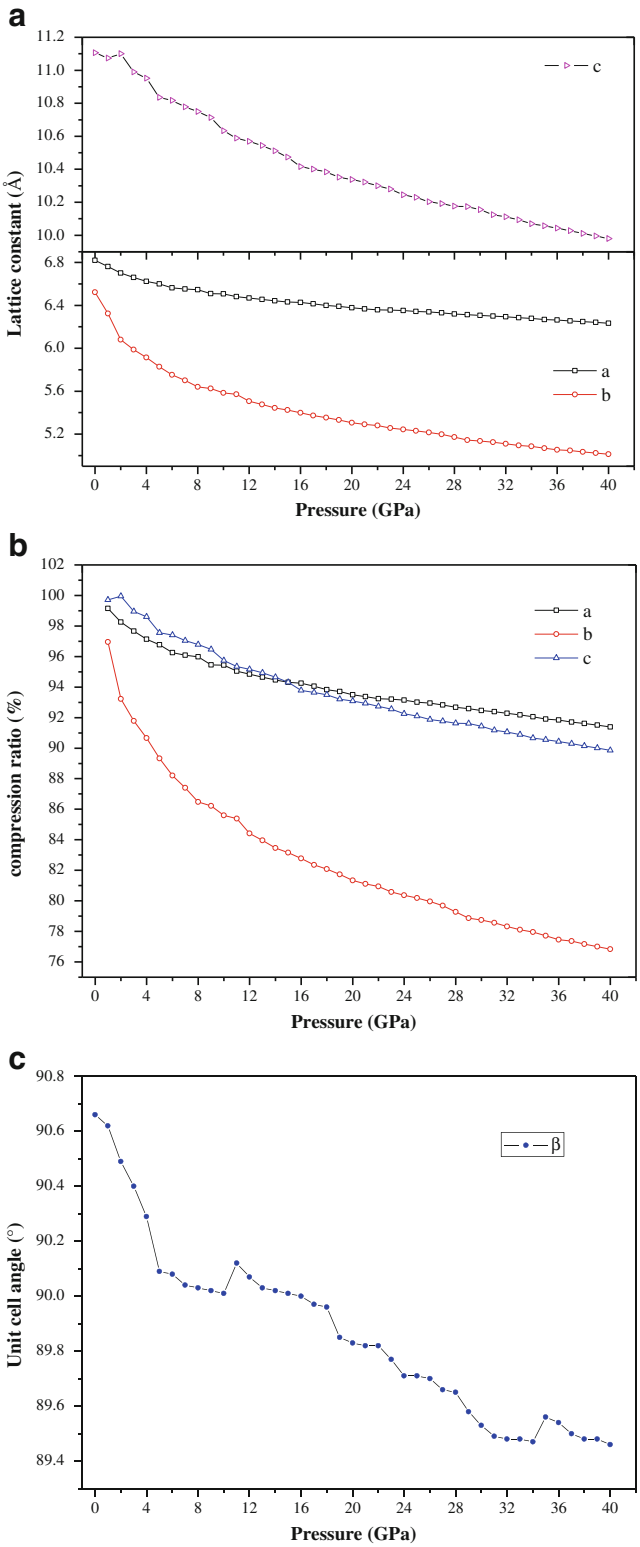

Fig. 2 Lattice constants, compression ratios, and unit cell angles of α-FOX-7 as a function of pressure

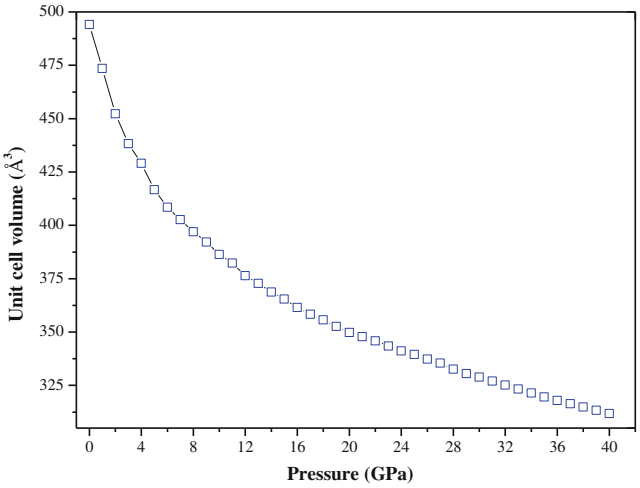

Fig. 3 Unit cell volumes of α-FOX-7 as a function of pressure

are higher than those of any other bond lengths, suggesting that the C-NO_2 bonds are more unstable than other bonds under compression and the C-NO_2 cleavage is possible to trigger the decomposition of α-FOX-7, consistent with experimental results [7, 12]. In addition, it is seen that the C1-C2 bond length decreases obviously at 2 GPa which may be caused by the structural transformation. As shown in Fig. 4b, the N1-O1, N1-O2, and N2-O3 bond lengths decrease gradually in the pressure range of 0–40 GPa, while the N2-O4 bond length increases gradually in 0–5 GPa but decreases very slowly until 40 GPa. The total decrease ratios for the four bond lengths are 1.03 %, 0.55 %, 1.12 %, and 0.08 %, respectively. The N3-H1 and N4-H4 bond lengths decrease very slowly with several tiny fluctuations in the pressure range of 0–40 GPa. The N3-H2 bond length decreases fast at 1 GPa but fluctuates between 1.041 and 1.043 Å in the pressure range of 1–25 GPa and then decreases gradually until 40 GPa. The N4-H4 bond length decreases in the pressure range of 0–10 GPa but increases at 11 and 12 GPa and then decreases gradually until 40 GPa. The total decrease ratios for the N3-H1, N3-H2, N4-H3, and N4-H4 bond lengths are 0.67 %, 0.95 %, 0.39 %, and 0.96 %, respectively. Overall, the decrease extent of the N-O and N-H bond lengths is much smaller than that of the C-C and C-N bond lengths. As shown in Fig. 4c, the average lengths of intramolecular H-bonds (H1-O1 and H3-O3 bonds) first decrease at 1 GPa but increase at 2 GPa. Then they keep unchanged in the range of 3–4 GPa but increase obviously at 5 GPa. In the pressure range of 6–10 GPa, they decrease very slowly but decrease fast at 11 GPa. Finally, they decrease till 40 GPa and do much more significantly at 29 GPa. In all, the intramolecular H-bonding interaction weakens at 2 and 5 GPa which may be caused by the structural transformations, but it strengthens with the increasing pressure up to 40 GPa. The average lengths of inter-molecular H-bonds (O2-H5, O2-H6, and O4-H6 bonds) decrease gradually in the pressure range of 0–40 GPa except for at 2–3 GPa and 29 GPa, in which they almost keep unchanged. The decrease trend of the average lengths of inter-molecular H-bonds indicates that

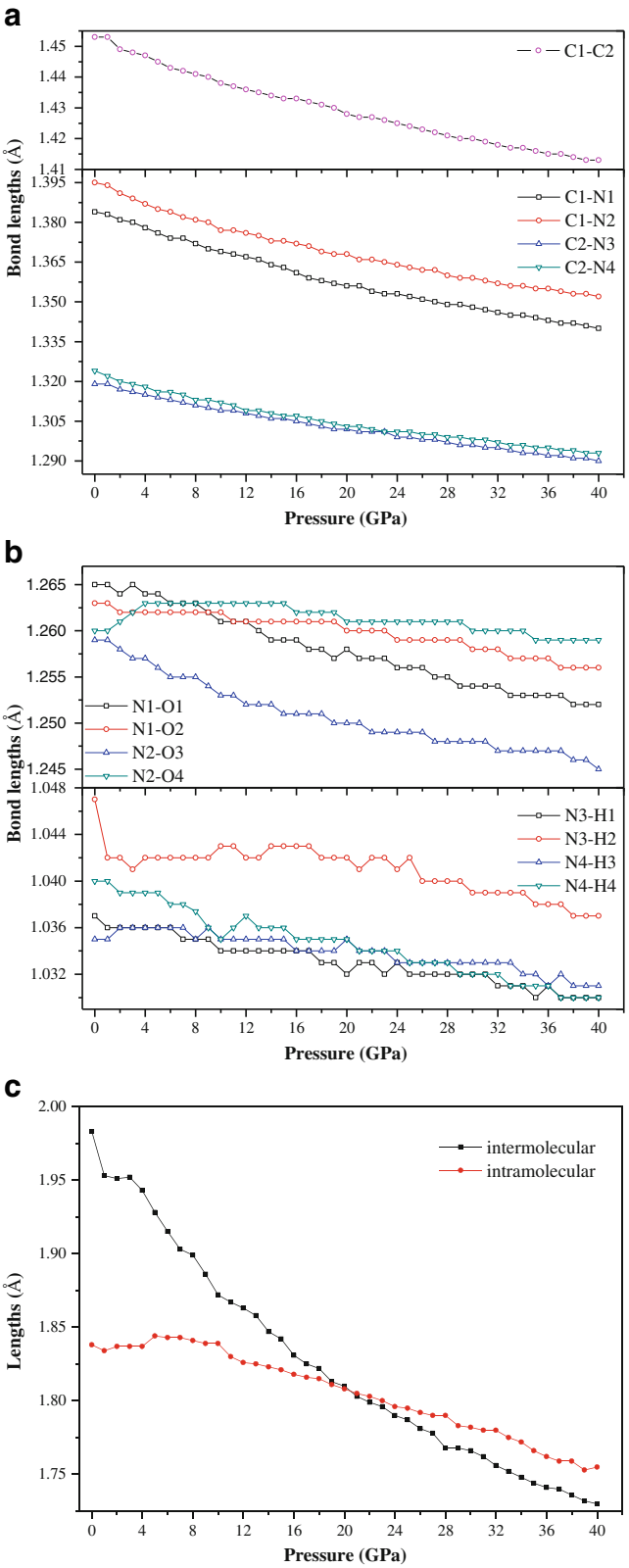

Fig. 4 Bond lengths of α-FOX-7 as a function of pressure

the inter-molecular H-bonding interaction strengthens with the increasing pressure.

Figure 5 displays several selected bond angles of α-FOX-7 at different pressures. At first, the N1-C1-C2 angle increases at 1 GPa but decreases at 2 GPa. Then, it increases until 10 GPa but decreases obviously at 11 GPa. In the pressure range of 12–18 GPa, it increases slowly but decreases at 19 GPa. Finally, it decreases until 40 GPa. The O1-N1-O2 angle increases at 1 GPa but decreases at 2 GPa and then decreases until 4 GPa but increases obviously at 5 GPa. The O3-N2-O4 angle decreases in the pressure range of 0–4 GPa but increases at 5 GPa, Then, it decreases until 14 GPa but increases obviously at 15 GPa. In the pressure range of 16–18 GPa, it increases gradually but decreases at 19 GPa. The H1-N3-H2 and H3-N4-H4 angles decrease at 1 GPa but increase at 2 GPa. Then, they decrease until 10 GPa but increase very obviously at 11 GPa. In the pressure range of 12–18 GPa, the H1-N3-H2 angle increases gradually, while the H3-N4-H4 angle decreases gradually. However, the H1-N3-H2 angle decreases suddenly, while the H3-N4-H4 angle increases at 19 GPa. The H1-N3-H2 angle fluctuates slightly in the pressure range of 20–34 GPa, but it decreases apparently at 35 GPa. The N2-C1-C2 angle decreases slowly in the pressure range of 0–4 GPa but decreases obviously at 5 GPa and then decreases fast until 40 GPa. The N3-C2-N4 angle increases at 1 GPa but decreases at 2 GPa. Then, it increases gradually in the pressure range of 12–40 GPa but more significantly at 19 and 35 GPa. In all, these irregular changes of the bond angles observed at 2, 5, 11, 19, and 35 GPa provide useful evidence on the structural transformations occurred at these pressures. In addition, the unexpected increase of O3-N2-O4 may suggest that there are also structural transformations at 11 and 15 GPa, respectively, which are in agreement with previous studies [22].

Figure 6 displays the twist angles of O1-N-O2 (in nitro group 1) and O3-N-O4 (in nitro group 2) against the C1-C2 bond in the *b*-*c* plane of α-FOX-7 at different pressures. It is

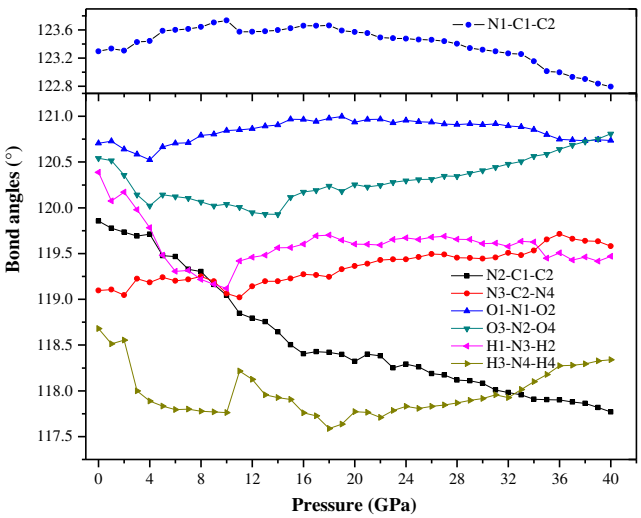

Fig. 5 Bond angles of α-FOX-7 as a function of pressure

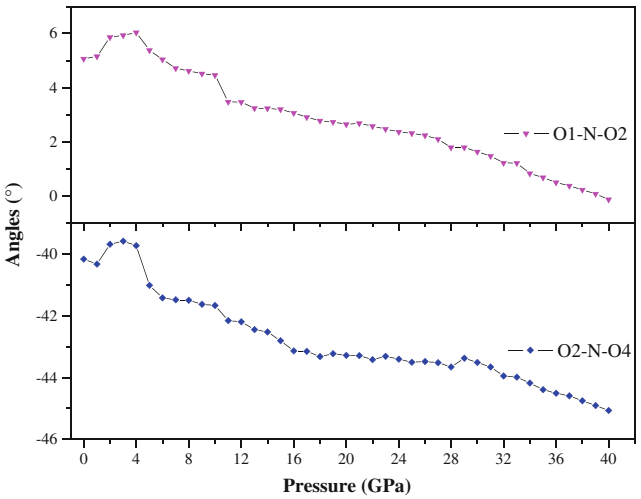

Fig. 6 Twist angles of O1-N-O2 (in nitro group 1) and O3-N-O4 (in nitro group 2) against the C1-C2 bond in the *b*-*c* plane of α-FOX-7 as a function of pressure

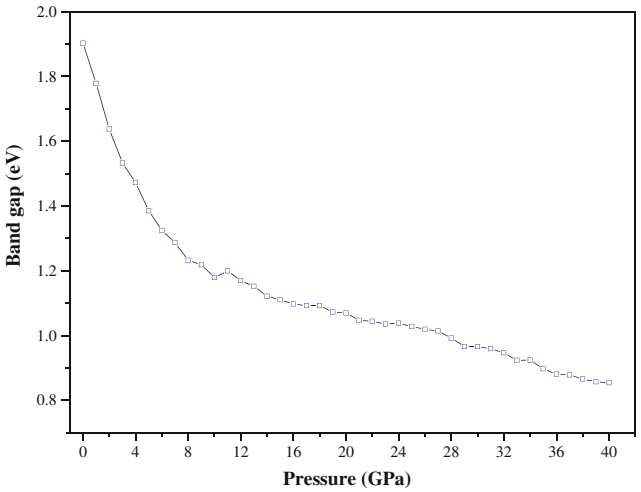

Fig. 7 Band gaps of α-FOX-7 as a function of pressure

seen that the two twist angles change irregularly at 2, 5, and 11 GPa, which are caused by the structural transformations. At 19, 35, or 15 GPa, there are no obvious unusual changes observed. However, the twist angle of nitro group 2 increases obviously at 29 GPa, suggesting that another structural transformation may occur at 29 GPa.

Overall, there may be six (or seven) structural transformations occurred at the pressure of 2, 5, 11, (15 GPa, possibly a completion of structural transformation), 19, 29, and 35 GPa, respectively. The former three (or four) structural transformations are in agreement with previous studies [22, 25], while the later three structural transformations are reported for the first time. These structural transformations are caused by the increasing of the interactions between different groups for the decreasing of intermolecular space under compression which help the crystal to bear the pressure without undergoing decomposition. Thus, strictly speaking, they cannot be called phase transitions. Further experimental and theoretical studies are needed to confirm these structural transformations.

Electronic structure

Band structure Figure 7 displays the band gaps of α-FOX-7 at different pressures. At first, the band gap decreases fast in the pressure range of 0–10 GPa but increases at 11 GPa suddenly. Then it decreases gradually until 40 GPa but does more obviously at 19, 29, and 35 GPa, respectively, which are caused by the structural transformations. Main reasons may be because the decrease of intermolecular space under compression can lead to an increase of the overlap of different groups of bands and hence to the increase of charge overlap and delocalization in the system. The variation degree of the band gap in different pressure ranges is different. The average decrease of the band gap in the pressure range of 0–10, 11–18, 19–28, 29–34, and 35–40 are 0.072, 0.013, 0.008, 0.003, and 0.007 eV/GPa, respectively. This shows that the band gap energy reduction is more pronounced in the low-pressure range compared to the high-pressure region. Previous studies reported that there is the relationship between the band gap and impact sensitivity for HMX [42], CL-20 [43], and heavy-metal azides [44]. That is, the smaller the band gap is, the easier the electron transfers from the valence bands to the conduction bands, and the more the materials become decomposed and exploded [45]. As shown in Fig. 7, the band gap of α-FOX-7 crystal gradually decreases with the increase of pressure except for the pressure of 11 GPa. Therefore, it may be inferred that the impact sensitivity for α-FOX-7 becomes more and more sensitive with the increment of pressure. An increase of the band gap for α-FOX-7 at 11 GPa shows that the new polymorph formed here is less sensitive than the former one.

Density of states Figure 8a displays the density of states (DOS) and partial DOS (PDOS) of α-FOX-7 at 0 GPa. The main features can be summarized as follows. (i) In the upper valence band, the PDOS of the N states of NH_2 and the C states are far larger that of the N states of NO_2. It may be inferred that the former makes more important contributions to the valence bands than the latter. This indicates that the N of NH_2 and C atoms act as an active center. (ii) Some strong peaks occur at the same energy in the PDOS of a particular C atom and a particular N atom of NH_2. It may be inferred that the two atoms are bonded strongly. Similarly, a particular C atom and a particular N atom of NO_2 are bonded strongly. (iii) In the conduction band region of DOS, the peaks are dominated by the C-p states, N-p states of NO_2, and N-p states of NH_2. Figure 8b–d presents the DOS of α-FOX-7 at 1, 2, 4, 5, 10, 11, 18, 19, 28, 29, 34, and 35 GPa. First, it is seen that the DOS peaks at 2, 5, 11, 29, and 35 GPa are similar to those at 1, 4, 10, 28, and 34 GPa, respectively. This

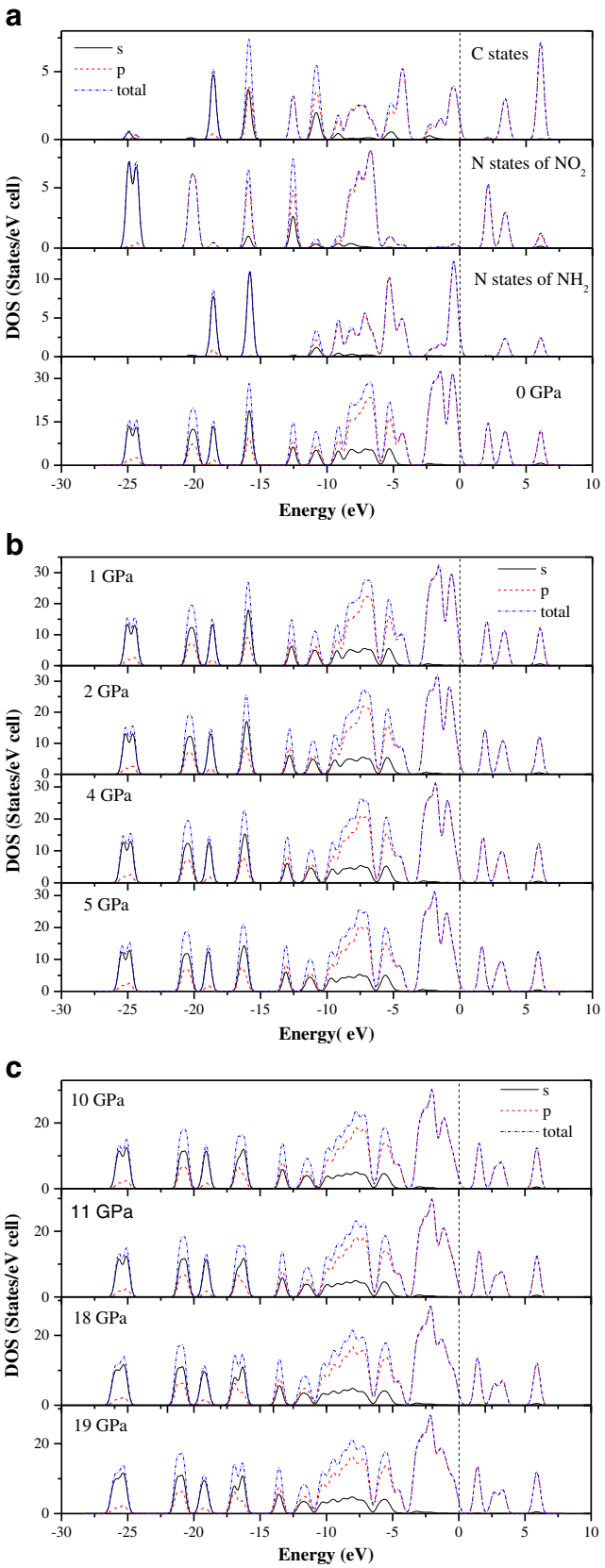

Fig. 8 Total and partial density of states (DOS) of **a** N states of NO_2, N states of NH_2, C states, and α-FOX-7 at 0 GPa; **b** DOS of α-FOX-7 at 1, 2, 4, and 5 GPa; **c** 10, 11, 18, and 19 GPa. **d** 28, 29, 34 and 35 GPa. The Fermi energy is shown as a *vertical dashed line*

shows that the structural transformations occurred at 2, 5, 11, 29, and 35 GPa have little effect on the DOS. Then, it is found that DOS peaks in the valence bands become more and more dispersed and have a tendency to shift to the lower energy with the increasing pressure. This indicates that the band splitting and dispersion increase accompanied with a broadening of DOS due to the enhanced intermolecular interactions at high pressures.

Absorption spectra

In this section, we intend to study the optical absorption coefficients of α-FOX-7 crystal at different pressures. The interaction of a photon with the electrons in the system can result in transitions between occupied and unoccupied states. The spectra resulting from these excitations can be described as a joint density of states between the valence and conduction bands. The imaginary part $\varepsilon_2(\omega)$ of the dielectric function can be obtained from the momentum matrix elements between the occupied and unoccupied wave functions within the selection rules, and the real part $\varepsilon_1(\omega)$ of dielectric function can be calculated from imaginary part $\varepsilon_2(\omega)$ by Kramer-Kronig relationship. Absorption coefficient $\alpha(\omega)$ can be evaluated from $\varepsilon_1(\omega)$ and $\varepsilon_2(\omega)$ [46].

$$\alpha(\omega) = \sqrt{2}\omega\left(\sqrt{\varepsilon_1^2(\omega) + \varepsilon_2^2(\omega)} - \varepsilon_1(\omega)\right)^{1/2} \quad (1)$$

The absorption coefficients $\alpha(\omega)$ of α-FOX-7 at different pressures are shown in Fig. 9. The absorption spectra are active over various regions corresponding to the molecular or lattice structures of the individual material. The evolution pattern of absorption spectra for α-FOX-7 at different pressures is qualitatively similar. They have an absorption band covering from 0 to 27.5 eV and more strong optical absorption from 1.5 to 12.5 eV. The magnitude of the absorption coefficients of these peaks allows an optical transition due to excitons. At ambient pressure, α-FOX-7 exhibits a relatively high absorption coefficient over a relatively few, closely spaced bands. The absorption bands from 12.5 to 16.0 eV correspond to the frequency of N-H stretching. The bands in the range from 1.5 to 12.4 eV overlap forming the strongest absorption region that corresponds to N-O vibration. The absorption bands from 16.1 to 20.0 eV correspond to the frequency of O-H stretching. It is seen that α-FOX-7 have higher absorption coefficients at high pressure than at low pressure in the frequency region of 0–16.0 eV, indicating that there is a shift toward higher frequencies in the absorption spectra and α-FOX-7 has relatively high optical activity at high pressure. Our calculated results here show that the absorption spectra of the α-FOX-7 crystal display a few strong bands in the fundamental absorption region at high pressure.

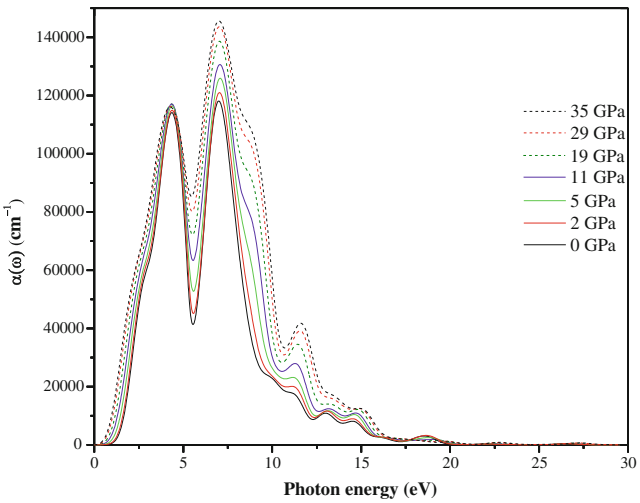

Fig. 9 Optical absorption spectra of α-FOX-7 at 0, 2, 5, 11, 19, 29, and 35 GPa

Thermodynamic properties

Figure 10 displays the calculated thermodynamic functions, including enthalpy (H), free energy (G), heat capacity (C_p), and entropy (S), as a function of temperature for crystalline α-FOX-7 at 0, 2, 5, 11, 19, 29, and 35 GPa. At ambient pressure, with the increase of temperature, the calculated enthalpies of α-FOX-7 monotonically increase. This is because the main contributions to the enthalpy are from the translations and rotations of the molecules at lower temperature, whereas the vibrational motion is intensified and makes more contributions to the enthalpy at higher temperature. For the free energy, the case is quite the contrary. As the temperature increases, its free energy value gradually decreases. As the pressure increases, H and G increase, while S and C_p decrease. At 298.15 K, the changes in the free energy of α-FOX-7 from 1 to 2 GPa, 4 to 5 GPa, 10 to 11 GPa, 18 to 19 GPa, 28 to 29 GPa, and 34 to 35 GPa, where structural transformations occur in α-FOX-7, are 3.27, 3.18,

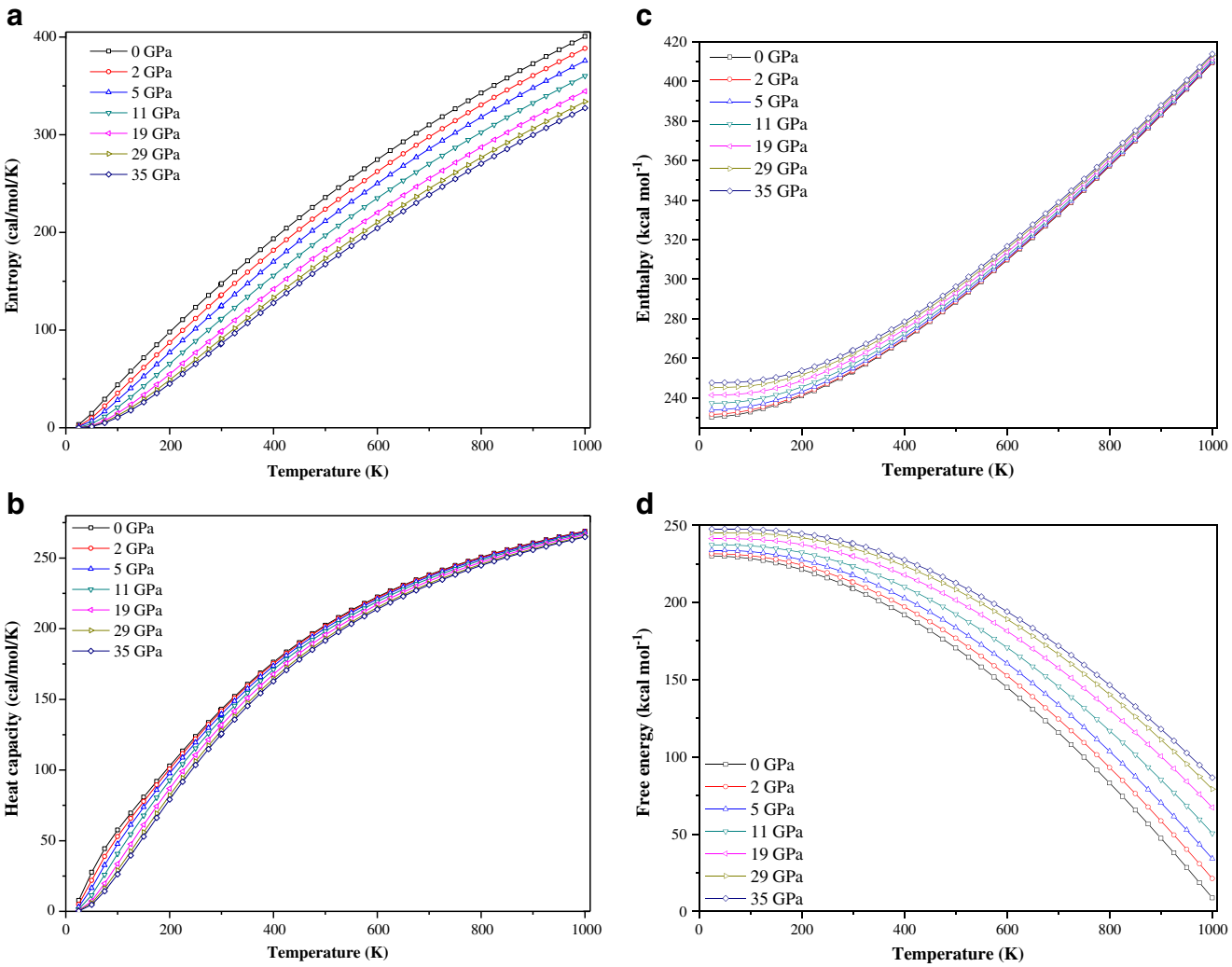

Fig. 10 Thermodynamic functions of α-FOX-7 at 0, 2, 5, 11, 19, 29, and 35 GPa

0.13, 1.04, 0.47, and 0.13 kcal mol^{-1}, respectively, whereas the changes for the enthalpy are 0.39, 0.78, 0.34, 0.48, 0.28, and 0.13 kcal mol^{-1}, respectively. This indicates that all of the structural transformations are endothermic and not spontaneous at room temperature.

Conclusions

In this work, DFT calculations have been performed to study the structural, electronic, absorption, and thermodynamic properties of crystalline α-FOX-7 in the pressure range of 0–40 GPa. A comprehensive analysis of the variation trends of the lattice constants, bond lengths, bond angles, and twist angles under compression show that there occur six structural transformations in α-FOX-7 at 2, 5, 11, 19, 29, and 35 GPa, respectively. The C1-N1 and C1-N2 bond lengths decrease much faster than any other bonds under compression, indicating that the C-NO_2 cleavage is possible to trigger the decomposition of α-FOX-7. The intra-molecular H-bonding interaction weakens at 2 and 5 GPa which may be caused by the structural transformations but strengthens with the increasing pressure up to 40 GPa. The decrease trend of the average lengths of inter-molecular H-bonds may indicate that the inter-molecular H-bonding interaction strengthens under compression.

As the pressure increases, the band gap of α-FOX-7 decreases fast in the pressure range of 0–10 GPa but increases at 11 GPa suddenly. Then, it decreases gradually until 40 GPa but does more obviously at 19, 29, and 35 GPa which are caused by the structural transformations. An analysis of density of states shows that the interactions between electrons, especially for the valence electrons, are strengthened under the influence of pressure. The absorption spectra show that α-FOX-7 has relatively high optical activity at high pressure. An analysis of thermodynamic properties indicates that all of the structural transformations are endothermic and not spontaneous at room temperature.

Acknowledgments This work was supported by the National Natural Science Foundation of China (Grant No. 21273115) and A Project Funded by the Priority Academic Program Development of Jiangsu Higher Education Institutions.

References

1. Bemm U, Östmark H (1998) Acta Crystallogr C: Cryst Struct Commun 54:1997–1999
2. Kjellstrom A, Latypov N, Eldsater C, Eriksson L (2005) FOI Swedish Defense Research Agency Technical Reprot No. SE-147 25 Tumba
3. Evers J, Klapötke TM, Mayer P, Oehlinger G, Welch JM (2006) Inorg Chem 45:4996–5007
4. Crawford MJ, Evers J, Göbel M, Klapötke TM, Mayer P, Oehlinger G, Welch JM (2007) Propell Explos Pyrot 32:478–495
5. Herve G, Jacob G, Latypov NV (2005) Tetrahedron 61:6743–6748
6. Peiris S, Wong C, Zerilli F, Russell T (2001) Shock Comp Cond Matter CP620:181–184
7. Hu A, Larade B (2006) Propell Explos Pyrot 31:355–360
8. Politzer P, Concha MC, Grice ME, Murray JS, Lane P (1998) J Mol Struct (THEOCHEM) 452:75–83
9. Gindulyte A, Massa L, Huang L, Karle J (1999) J Phys Chem A 103:11045–11051
10. Ji GF, Xiao HM, Dong HS, Gong XD, Li JS, Wang ZY (2001) Acta Chim Sin 59:39–47
11. Sorescu DC, Boatz JA, Thompson DL (2001) J Phys Chem A 105:5010–5021
12. Ju XH, Xiao HM, Xia QY (2003) J Chem Phys 119:10247–10255
13. Gilardi R (1999) CCCD 127539, Cambridge Structural Database, Cam-bridge Crystallographic Data Center, Cambridge, UK
14. Zerilli FJ, Kuklja M (2007) J Phys Chem A 111:1721–1725
15. Trzciński WA, Cudziło S, Chyłek Z, Szymańczyk L (2008) J Hazard Mater 15:605–612
16. Zerilli FJ (2006) J Phys Chem A 110:5173–5179
17. Fabbiani FPA, Pulham CR (2006) Chem Soc Rev 35:932–942
18. Cady HH, Smith LC (1961) Los Alamos Scientific Laboratory Repot LAMS-2653 TID-4500; Los Almos National Laboratory: Los Alamos, NM
19. Main P, Cobbledic RE, Small RWH (1985) Acta Crystallogr Sect C 41:1351–1354
20. Dreger ZA, Gupta YM (2010) J Phys Chem A 114:8099–8105
21. Dreger ZA, Gupta YM (2007) J Phys Chem B 111:3893–3903
22. Pravica M, Liu Y, Robinson J, Velisavljevic N, Liu ZX, Galley M (2012) J Appl Phys 111:103524–103529
23. Peiris S, Wong C, Zerilli F (2004) J Chem Phys 120:8060–8066
24. Peiris S, Wong C, Kuklja M, Zerilli F (2002) 12th Int Deton Symp Pro, pp 12.0617-12.0624
25. Brangham J, Pravica M, Galley M (2011) Undergergraduate Research Opportunities Program (UROP). pp 23 http://diaitalscholarship.unlv.edu/cs_urop/2011/aug9/23
26. Zhao J, Liu H (2008) Comput Mater Sci 42:698–703
27. Zhu WH, Zhang XW, Wei T, Xiao HM (2009) Theor Chem Acc 124:179–186
28. Zhu WH, Zhang XW, Zhu W, Xiao HM (2008) Phys Chem Chem Phys 10:7318–7323
29. Zhu WH, Xiao JJ, Xiao HM (2006) Chem Phys Lett 422:117–121
30. Zhu WH, Xiao HM (2006) J Phys Chem B 110:18196–18203
31. Segall MD, Lindan PJD, Probert MJ, Pickard CJ, Hasnip PJ, Clark SJ, Payne MC (2002) J Phys Condens Matter 14:2717–2744
32. Vanderbilt D (1990) Phys Rev B 41:7892–7895
33. Kresse G, Furthmüller J (1996) Phys Rev B 54:11169–11186
34. Fletcher R (1980) Practical methods of optimization, vol 1. Wiley, New York
35. Ceperley DM, Alder BJ (1980) Phys Rev Lett 45:566–569
36. Perdew JP, Zunger A (1981) Phys Rev B 23:5048–5079
37. Yoo C-S, Cynn H (1999) J Chem Phys 111:10229–10235
38. Gump JC, Peiris SM (2005) J Appl Phys 97:053513
39. Zhu WH, Xiao HM (2009) J Phys Chem B 113:10315–10321
40. Zhu WH, Wei T, Zhu W, Xiao HM (2008) J Phys Chem A 112:4688–4693
41. Perdew JP, Chevary JA, Vosko SH, Jackson KA, Pederson MR, Singh DJ, Fiolhais C (1992) Phys Rev B 46:6671–6687
42. Zhu WH, Xiao JJ, Ji GF, Zhang F, Xiao HM (2007) J Phys Chem B 111:12715–12722
43. Xu XJ, Zhu WH, Xiao HM (2007) J Phys Chem B 111:2090–2097
44. Zhu WH, Xiao HM (2008) J Comput Chem 29:176–184
45. Zhu WH, Xiao HM (2010) Struct Chem 21:657–665
46. Saha S, Sinha TP, Mookerjee A (2000) Phys Rev B 62:8828–8834